Chemical Research in Toxicology

Article

pubs.acs.org/crt

Structures of (5′*S*)-8,5′-Cyclo-2′-deoxyguanosine Mismatched with dA or dT

Hai Huang,[†] Rajat S. Das,[‡] Ashis K. Basu,[‡] and Michael P. Stone*,[†]

[†]Department of Chemistry, Center in Molecular Toxicology, and Center for Structural Biology, Vanderbilt-Ingram Cancer Center, Vanderbilt University, Nashville, Tennessee 37235, United States

[‡]Department of Chemistry, University of Connecticut, Storrs, Connecticut 06269, United States

Supporting Information

ABSTRACT: Diastereomeric 8,5′-cyclopurine 2′-deoxynucleosides, containing a covalent bond between the deoxyribose and the purine base, are induced in DNA by ionizing radiation. They are suspected to play a role in the etiology of neurodegeneration in xeroderma pigmentosum patients. If not repaired, the *S*-8,5′-cyclo-2′-deoxyguanosine lesion (*S*-cdG) induces Pol V-dependent mutations at a frequency of 34% in *Escherichia coli*. Most are *S*-cdG → A transitions, suggesting mis-incorporation of dTTP opposite the lesion during replication bypass, although low levels of *S*-cdG → T transversions, arising from mis-incorporation of dATP, are also observed. We report the structures of 5′-d(GTGCXTGTTTGT)-3′·5′-d(ACAAACAYGCAC)-3′, where X denotes *S*-cdG and Y denotes either dA or dT, corresponding to the situation following mis-insertion of either dTTP or dATP opposite the *S*-cdG lesion. The *S*-cdG·dT mismatch pair adopts a wobble base pairing. This provides a plausible rationale for the *S*-cdG → A transitions. The S-cdG·dA mismatch pair differs in conformation from the dG·dA mismatch pair. For the *S*-cdG·dA mismatch pair, both *S*-cdG and dA intercalate, but no hydrogen bonding is observed between *S*-cdG and dA. This is consistent with the lower levels of *S*-cdG → T transitions in *E. coli*.

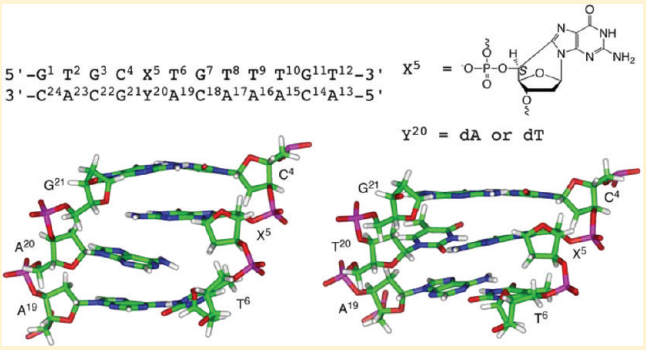

INTRODUCTION

Hydroxyl radicals, generated by cellular oxidative stress and inflammation, damage nucleobases[1] or deoxyribose sugars,[2] or both in DNA.[3] At 2′-deoxyguanosines, hydroxyl radical-mediated hydrogen abstraction at the deoxyribose C5′-position followed by attack at the guanine C8 carbon forms an N7-centered radical, which may be oxidized to diastereomeric 8,5′-cyclo-2′-deoxyguanosines (cdG).[4−10] The 8,5′-cyclo-2′-deoxyadenosines (cdA) have also been characterized.[3,6,8−15] These 8,5′-cyclopurine-2′-deoxynucleosides have been detected at the nucleotide level,[4,11] in DNA,[4,16−18] and cells in vitro,[5] in human urine,[19] and in vivo.[18,20,21] They might contribute to neurologic disease in xeroderma pigmentosum complementation group C (XP-C) patients.[22] They are also believed to play roles in Cockayne syndrome,[18] breast and ovarian cancer,[20] and familial Mediterranean fever.[23]

It has been reported that *S*-cdG does not block primer elongation by Klenow DNA polymerases, and dATP is preferentially incorporated opposite the lesion in vitro.[25] However, in *Escherichia coli*, *S*-cdG blocks DNA replication and is refractory to repair.[24] Upon induction of the SOS response, it induces 34% mutations.[24] Most are *S*-cdG → A transitions, although *S*-cdG → T transversions and low levels of deletions of the 5′-neighbor dC are also observed.[24]

For both cdG and cdA, the diastereomeric ratio at the C5′-position depends on experimental conditions and DNA conformation.[4−6,13,19,26,27] Computational studies predicted that the incorporation of the cdA stereoisomers into DNA would result in helical distortions at the lesion site.[28−30] Both the *R*- and the *S*-diastereomers of the 8,5′-cA ribonucleoside have been crystallized, and both exhibit the *anti* conformation about the N-glycosidic bond with $\chi_{O4'-C1'-N9-C8}$ = 30 or 27°, respectively.[31,32] The fused six-member ring C8−N9−C1′−O4′−C4′−C5′ adopts the half-chair conformation with the O4′ and C4′ out of plane. The ribose adopts the O4′-*exo* ($_0$T^1) pseudorotation with P = 289° and τ_m = 48°. Molecular mechanics calculations predicted that the cdA diasetereomers maintain the O4′-*exo* pseudorotation when placed opposite dT in DNA.[28] The NMR data and ab initio calculations suggest that incorporation of the *S*-cdA into di- or trinucleotides does not change the O4′-*exo* pseudorotation.[33]

Recently, we reported the structure of the *S*-cdG·dC pair in 5′-d(GTGCXTGTTTGT)-3′·5′-d(ACAAACACGCAC)-3′, containing the DNA sequence of *p53* codons 272−275 (X = *S*-cdG, Scheme 1).[34] The *S*-cdG participates in Watson−Crick hydrogen bonding with the complementary dC. However, the

Received: November 22, 2011
Published: February 6, 2012

Scheme 1. Numbering Scheme of the Mismatched Oligodeoxynucleotide Duplexes Containing the *S*-cdG

5′-G^{1} T^{2} G^{3} C^{4} X^{5} T^{6} G^{7} T^{8} T^{9} $T^{10}G^{11}T^{12}$-3′
3′-$C^{24}A^{23}C^{22}G^{21}Y^{20}A^{19}C^{18}A^{17}A^{16}A^{15}C^{14}A^{13}$-5′

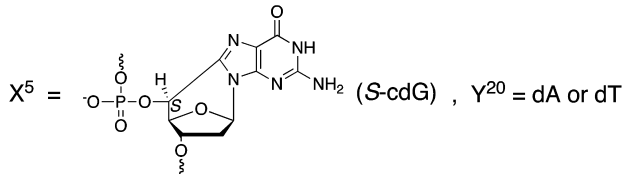

S-cdG deoxyribose shifts to the O4′-*exo* pseudorotation with $P = 280°$. This altered backbone torsion angles γ from ∼50 to −67° and δ from ∼120 to 149°, as compared with canonical B-DNA. Additionally, the torsion angles β and χ are changed from ∼180 to −87° and from ∼−120 to −157°, respectively. The twist and base pair shift helicoidal parameters are perturbed at the $C^{4}{\cdot}G^{21}$ and $X^{5}{\cdot}C^{20}$ base pairs. The purine ring is *anti* about the N-glycosidic bond, and the fused six-membered ring adopts the half-chair conformation with O4′ and C4′ out of plane.

Here, we report the structures of the duplexes 5′-d(GTGCXTGTTTGT)-3′·5′-d(ACAAACAYGCAC)-3′ (X denotes *S*-cdG; Y denotes either dA or dT, Scheme 1). These model the situation following mis-incorporation of dTTP opposite *S*-cdG, leading to *S*-cdG → A transitions, or following mis-incorporation of dATP opposite *S*-cdG, leading to *S*-cdG → T transversions in *E. coli*.[24] The *S*-cdG·dT mismatch pair adopts a wobble base pairing, providing a plausible rationale for the *S*-cdG → A transitions. For the *S*-cdG·dA mismatch pair, both *S*-cdG and dA intercalate, but no hydrogen bonding is observed between *S*-cdG and dA. This is consistent with the lower levels of *S*-cdG → T transitions in *E. coli*.[24]

MATERIALS AND METHODS

Materials. The oligodeoxynucleotide 5′-d(GTGCXTGTTTGT)-3′ (X = *S*-cdG) was synthesized and characterized as reported.[34] The oligodeoxynucleotides 5′-d(GTGCGTGTTTGT)-3′ and 5′-d(ACAAACAYGCAC)-3′ (Y = dA or dT) were synthesized and purified by anion-exchange chromatography (Midland Certified Reagent Co., Midland, TX). Oligodeoxynucleotides were desalted using Sephadex G-25. The oligodeoxynucleotides 5′-d(GTGCGTGTTTGT)-3′ or 5′-d(GTGCXTGTTTGT)-3′ were annealed at 1:1 stoichiometry with the complementary oligodeoxynucleotide 5′-d(ACAAACAYGCAC)-3′ in 10 mM NaH_2PO_4, 100 mM NaCl, and 50 μM Na_2EDTA (pH 7.0). The solutions were heated to 95 °C for 10 min and cooled to room temperature. The duplexes were isolated using DNA grade hydroxylapatite with a gradient from 10 to 200 mM NaH_2PO_4 in 100 mM NaCl and 50 μM Na_2EDTA (pH 7.0) and desalted using Sephadex G-25.

Melting Temperature. Melting temperatures of the DNA duplexes were measured by UV/vis spectroscopy at 260 nm in 10 mM NaH_2PO_4, 100 mM NaCl, and 50 μM Na_2EDTA (pH 7.0). The strand concentration was 10 μM. The thermal scans proceeded from 10 to 80 °C with an interval of 1 °C. The melting temperatures were calculated by differentiating the absorbance vs temperature profiles.

NMR. Samples were at 1.0 mM strand concentration. Samples for the nonexchangeable protons were dissolved in 500 μL in 10 mM NaH_2PO_4, 100 mM NaCl, and 50 μM Na_2EDTA (pH 7.0). They were exchanged with D_2O and suspended in 280 μL of 99.996% D_2O, and the pH was adjusted with dilute DCl or NaOD. Experiments were performed at 800 MHz. The temperature was 25 °C. Magnitude correlated spectroscopy (COSY) spectra were recorded with 512 real data in the t1 dimension and 2048 real data in the t2 dimension. Total correlation spectroscopy (TOCSY) spectra were recorded with a mixing time of 80 ms. Chemical shifts were referenced to water. The exclusive correlation spectroscopy (E-COSY) spectra were recorded with 1024 real points in the t1 dimension and 4096 real points in the t2 dimension.[35] The spectra were zero-filled during processing to create a matrix of 2048 × 16384 points. The temperature was 30 °C. Nuclear Overhauser effect spectroscopy (NOESY) spectra were recorded with 512 real points in the t1 dimension and 2048 real points in the t2 dimension. NOESY spectra were zero-filled during processing to create a matrix of 1024 × 1024 real points. NOESY experiments used time-proportional phase increment (TPPI) quadrature detection[36] and mixing times of 60, 150, 200, and 250 ms. The relaxation delay was 1.5 s. Data were processed using the program TOPSPIN[37] and analyzed with the program SPARKY.[38] Samples for the observation of exchangeable protons were dissolved in 500 μL of 10 mM NaH_2PO_4 and 100 mM NaCl, 50 μM EDTA (pH 7.0) containing 9:1 H_2O:D_2O (v/v) (pH 7.0). NOESY experiments were performed at 500 MHz, at 5 °C. The Watergate sequence was used for water suppression,[39] with a nuclear Overhauser enhancement (NOE) mixing time of 250 ms. The $^{31}P-H^{1}$ experiments were carried out at the ^{1}H frequency of 600 MHz. $^{31}P-H3'$ ^{3}J couplings were applied to determine the phosphodiester backbone conformation.[40] ^{31}P chemical shifts were referenced using indirect shift ratios.[41]

Distance and Dihedral Angle Restraints. Integration footprints were defined using NOE cross-peaks obtained at a mixing time of 250 ms. NOE intensities from data obtained at mixing times of 60, 150, 200, and 250 ms to check for the presence of spin diffusion effects were determined by volume integrations. For each mixing time, these were combined as necessary with intensities generated from complete relaxation matrix analysis of a starting structure to yield a hybrid NOE intensity matrix.[42,43] The program MARDIGRAS[44−46] iteratively refined the hybrid intensity matrix and optimized agreement between calculated and experimental NOE intensities. The RANDMARDI algorithm[45] carried out iterations, randomizing peak volumes within limits specified by the input noise level.[46] Calculations were initiated using isotropic correlation times of 2, 3, and 4 ns. Analysis of these data yielded distance restraints used in restrained molecular dynamics (rMD) calculations (Table S3 in the Supporting Information) and the corresponding standard deviations for the distance restraints.

The pseudorotations (P) were estimated by examining the $^{3}J_{HH}$ of deoxyribose protons.[47] The data were fit to curves relating the coupling constants to P, deoxyribose pucker amplitude (ϕ), and the percentage S type conformation. The P and ϕ ranges were converted to the dihedral angles $\nu_0-\nu_4$. To obtain backbone torsion angle restraints for the modified, flanking, and terminal base pairs, coupling constants measured from $^{1}H-^{31}P$ heternuclear multiple bond correlation spectroscopy (HMBC) spectra were applied[48,49] to the Karplus relationship[50] to determine the dihedral angle ε (C4′−**C3′**−**O3′**−P), related to the H3′−**C3′**−**O3′**−P angle by a 120° shift. The ζ (C3′−**O3′**−**P**−O5′) torsion angles were calculated from the correlation between ε and ζ in B-DNA.[40] At all other base pairs, backbone torsion angle restraints utilized canonical values derived from B-DNA.[51] Watson−Crick hydrogen-bonding restraints minimized propeller twisting between base pairs, except at the $X^{5}{\cdot}T^{20}$ base pair in the *S*-cdG·dT mismatched duplex and at the $X^{5}{\cdot}A^{20}$ and $A^{6}{\cdot}T^{19}$ base pairs in the *S*-cdG·dA mismatched duplex.

Molecular Dynamics Calculations. The partial charges for the cdG nucleotide were obtained from density functional theory (DFT) calculations, utilizing the B3LYP/6-31G* basis set and the program GAUSSIAN.[52] The starting structures were generated from A and B type DNAs by constructing a bond between G5 C8 and G^{5} C5′ followed by 200 iterations of potential energy minimization using the conjugate gradients algorithm. The rMD calculations utilized a simulated annealing approach.[53] The calculations were conducted with the program AMBER[54] and the parm99 force field. The generalized Born (GB) model[55] with parameters developed by Tsui and Case[56] was used for implicit water simulation. The program complete relaxation matrix analysis (CORMA) was utilized to calculate the NOE intensities from the structures emergent from calculations. Helicoidal analyses were carried out with the programs CURVES[57] and 3DNA.[58]

dx.doi.org/10.1021/tx2005053 | *Chem. Res. Toxicol.* 2012, 25, 478−490

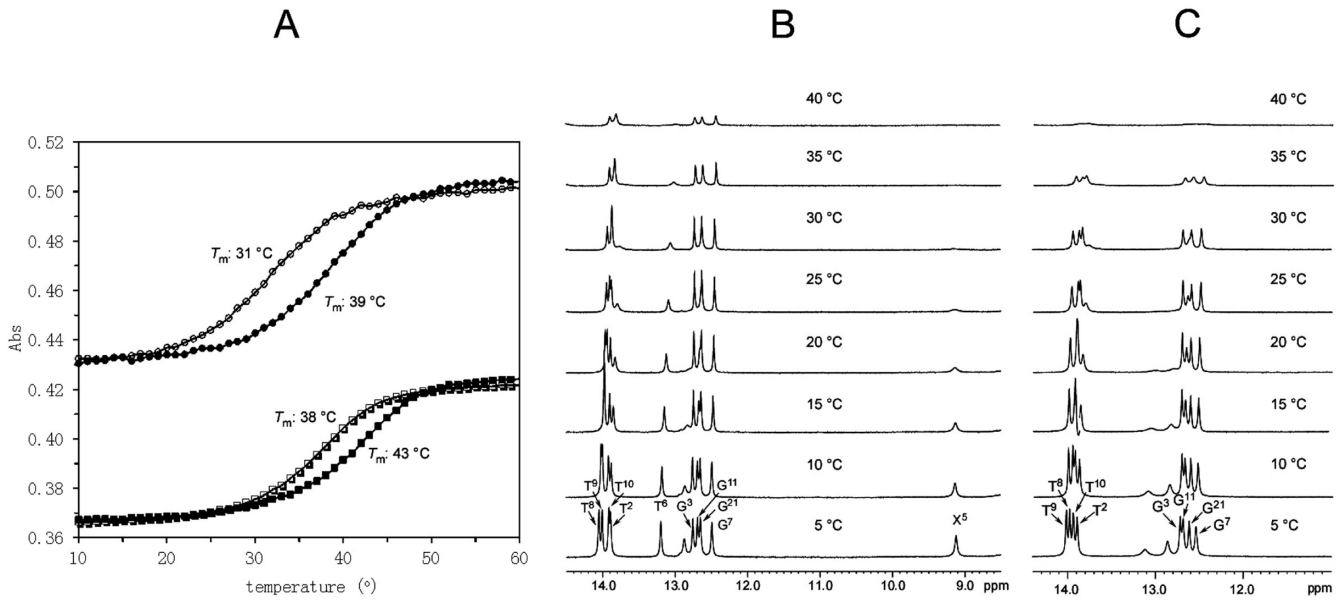

Figure 1. (A) UV melting profiles of the mismatched duplexes as compared with the corresponding unmodified duplexes: duplex containing dG·dA base pair (○), duplex containing *S*-cdG·dA base pair (●), duplex containing dG·dT base pair (□), and duplex containing *S*-cdG·dT base pair (■). (B) ^{1}H NMR of the mismatched duplex containing the *S*-cdG·dT base pair at different temperatures. (C) ^{1}H NMR of the mismatched duplex containing the *S*-cdG·dA base pair at different temperatures. The broad resonance at ~13.1 ppm observed at 5−15 °C was unassignable; it might be assigned to X^5 N1H or T^6 N3H.

RESULTS

Thermal Stability. The duplex containing the *S*-cdG·dT base pair exhibited a melting temperature (T_m) of 38 ± 1 °C. The unmodified dG·dT mismatched duplex exhibited a T_m of 43 °C under the same conditions (Figure 1A). Thus, the incorporation of *S*-cdG reduced the T_m by 5 °C. The duplex containing the *S*-cdG·dA pair exhibited a T_m of 31 ± 1 °C. The unmodified dG·dA mismatched duplex exhibited a T_m of 39 ± 1 °C (Figure 1A). Thus, the incorporation of *S*-cdG reduced the T_m by 8 °C. ^{1}H NMR spectra of the duplex containing the *S*-cdG·dT pair were compared with the unmodified mismatched duplex at different temperatures (Figure 1B). At the X^5·T^{20} base pair, the T^{20} N3H resonance was not observed at 5 °C. For the modified duplex, the T^6 N3H resonance broadened at lower temperature than did the other thymine imino resonances. ^{1}H NMR spectra of the duplex containing the *S*-cdG·dA base pair at different temperatures are displayed in Figure 1C. The X^5 and T^6 imino resonances were not observed at 5 °C. The imino resonances for base pairs C^4·G^{21}, G^5·A^{20}, and T^6·A^{19} of the unmodified duplex were not observed. Moreover, for the unmodified duplex containing the G^5·A^{20} mismatch, the C^4 and C^{18} H5 → H6 scalar couplings were not observed, and that of C^{22} was weak.

***S*-cdG Mismatched with dT.** *NMR Resonance Assignments.* The nonexchangeable protons of the *S*-cdG-modified duplex were assigned based upon the NOE sequential connectivity of the base proton H6 or H8 dipolar couplings with H1′ deoxyribose protons (Figure 2A,B).[59,60] For the modified strand, the sequential connectivity was observed from G^1 to C^4. Because the *S*-cdG nucleotide lacked a proton at the C8 carbon, the sequential connectivity exhibited an interruption at X^5. The X^5 H1′ proton was identified at 6.11 ppm; it exhibited a weak X^5 H1′ → T^6 H6 NOE. The sequential connectivity resumed from T^6 to T^{12}. For the modified strand, all of the deoxyribose H1′ protons were observed within a narrow chemical shift window, between 5.8 and 6.3 ppm. The complete sequential connectivity was observed for the complementary strand.

The assignments of X^5 deoxyribose protons were made by analysis of scalar and dipolar couplings. Figure 3A displays a tile plot derived from a NOESY spectrum obtained at 60 ms mixing time. X^5 H1′ exhibited dipolar couplings with H2′ and H2″; weak scalar couplings were also observed. H3′ exhibited dipolar couplings with H2′, H2″, and H4′, whereas the scalar couplings were not observed. H4′ exhibited both scalar and dipolar couplings with the H5′ proton. The geminal H2′ and H2″ protons were not resolved. For the remainder of the duplex, the H2′, H2″, H3′, and H4′ deoxyribose resonances were unequivocally assigned. The absolute configurations of the geminal H2′ and H2″ protons were assigned from their NOEs to H1′ and H3′. With the exception of the unresolved resonances for X^5, G^{11}, and T^{12}, H2′ exhibited a weaker NOE with H1′ than did H2″, whereas it exhibited a stronger NOE with H3′ than did H2″. The resonance assignments of the nonexchangeable DNA protons are tabulated in Table S1 in the Supporting Information.

The resonances of the base imino protons were assigned based on sequential connectivity in NOESY spectra, and the assignments were supported by NOEs to the amino protons of Watson−Crick base pairs (Figure 4A).[61] The NOE sequential connectivity was observed from T^2 → G^3 to G^{21} and from T^6 → G^7 → T^8 → T^9 → T^{10} to G^{11}. At the 5′-neighbor base pair, G^{21} N1H exhibited NOEs with C^4 N^4 H1 and N^4 H2. At the 3′-neighbor base pair, the T^6 N3H resonance exhibited NOEs with A^{19} H2 and A^{19} N^6 H1. With the exception of the terminal base pairs, the remaining NOEs arising from Watson−Crick hydrogen bonding were observed. The X^5 N1H resonance was observed at ~9.1 ppm. It exhibited an NOE with X^5 N^2H, which also had an NOE with T^6 N3H (Figure 4B). As compared to other guanine imino resonances, X^5 N1H shifted upfield.

Deoxyribose Coupling Constants. The scalar couplings of the 2′-deoxyribose H1′ protons with the H2′ and H2″ protons

dx.doi.org/10.1021/tx2005053 | *Chem. Res. Toxicol.* 2012, 25, 478−490

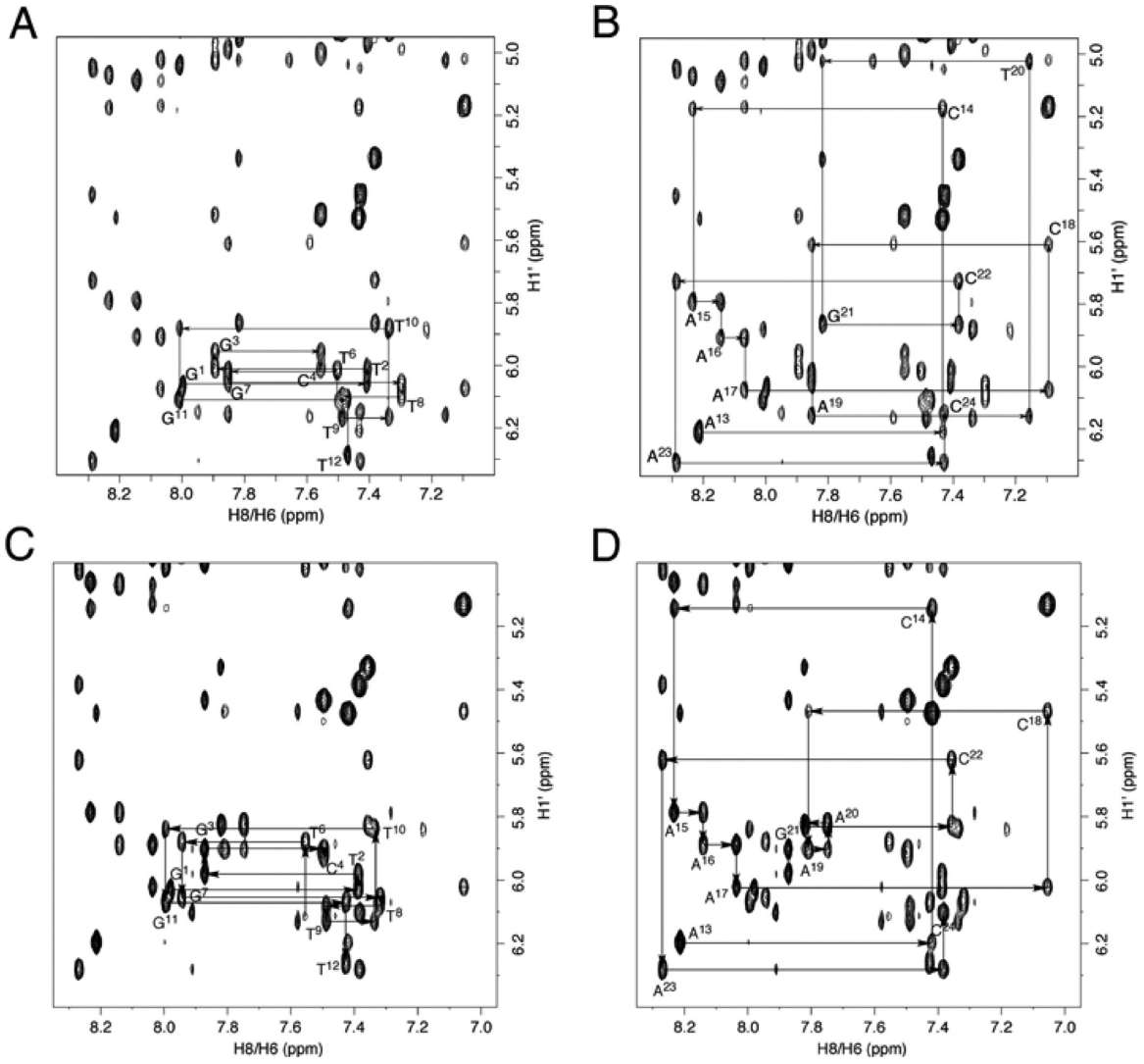

Figure 2. NOE (250 ms) connectivities of base H8/H6 protons with deoxyribose H1′ protons of the *S*-cdG modified duplexes. (A) Modified strand for the duplex containing the *S*-cdG·dT base pair. (B) Complementary strand for the duplex containing the *S*-cdG·dT base pair. (C) Modified strand for the duplex containing the *S*-cdG·dA base pair. (D) Complementary strand for the duplex containing the *S*-cdG·dA base pair.

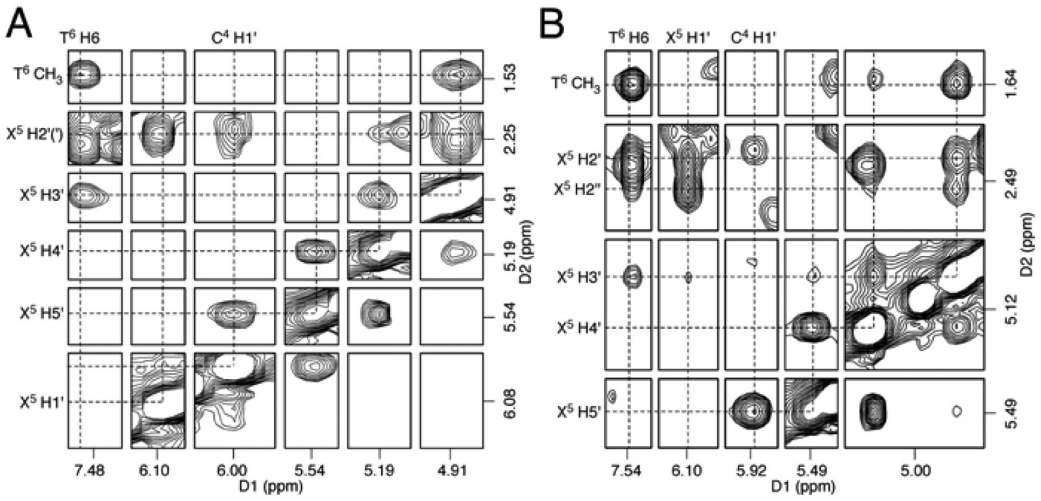

Figure 3. Expansions of NOESY spectra (60 ms) showing the assignment of *S*-cdG nonexchangeable protons. (A) Duplex containing *S*-cdG·dT base pair. (B) Duplex containing *S*-cdG·dA base pair.

were measured from an E-COSY spectrum (Figure S1 in the Supporting Information). The $^{3}J_{H1'-H2'}$ and $^{3}J_{H1'-H2''}$ values for X^{5} were 2.1 and 4.9 Hz, respectively. The $^{3}J_{H4'-H5'}$ was 4.9 Hz, whereas the $^{3}J_{H3'-H4'}$ was not measurable. For T^{20}, $^{3}J_{H1'-H2'}$ and

dx.doi.org/10.1021/tx2005053 | *Chem. Res. Toxicol.* 2012, 25, 478−490

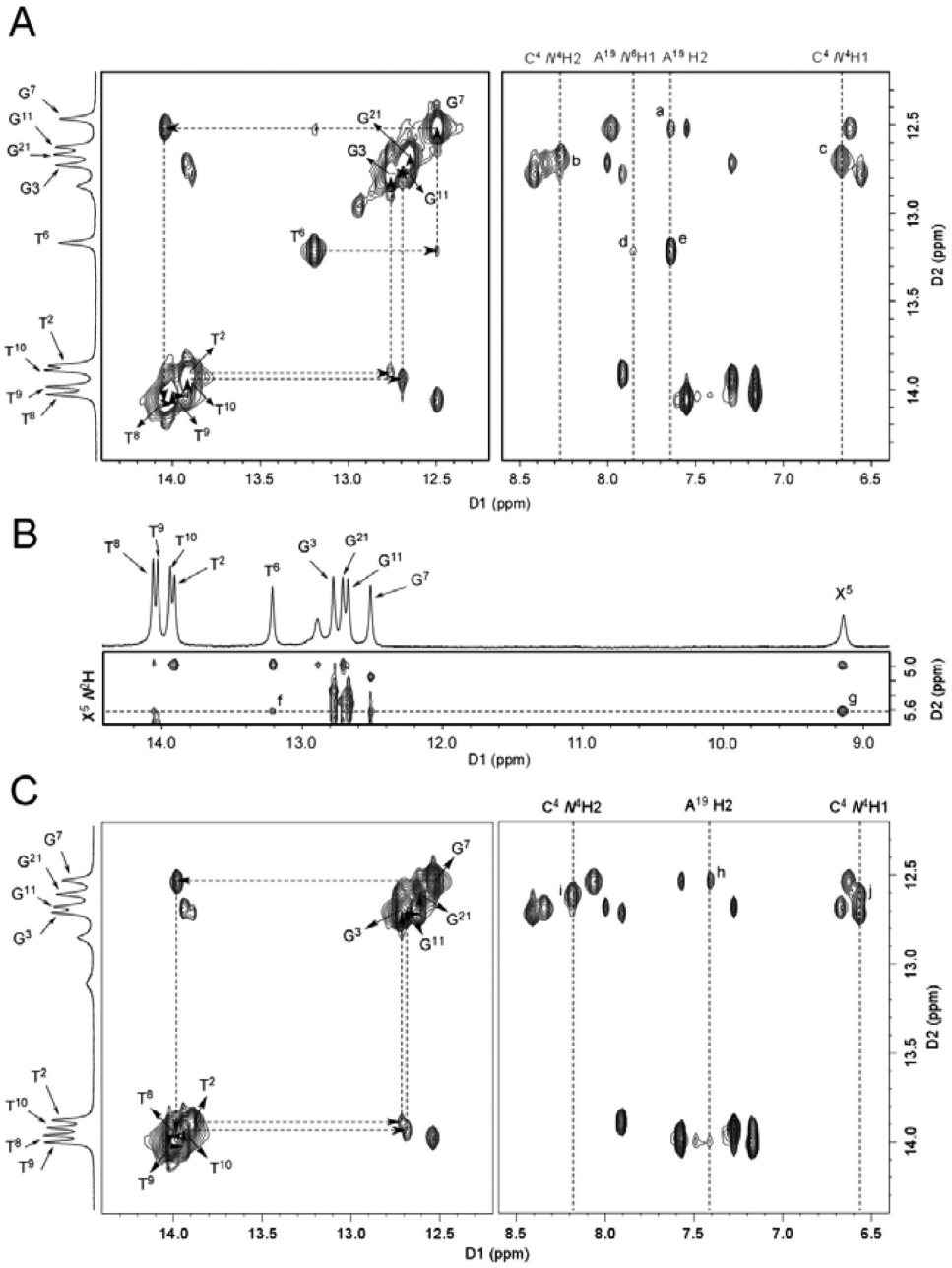

Figure 4. Assignment of the exchangeable protons of the *S*-cdG modified duplexes. (A) Duplex containing the *S*-cdG·dT base pair; NOE cross-peaks are assigned as follows: a, A^{19} H2 → G^{7} N1H; b, C^{4} N^{4}H2 → G^{21} N1H; c, C^{4} N^{4}H1 → G^{21} N1H; d, A^{19} N^{6} H1 → T^{6} N3H; and e, A^{19} H2 → T^{6} N3H. (B) Assignment of X^{5} N1H in the duplex containing the *S*-cdG·dT base pair; NOE cross-peaks are assigned as follows: f, T^{6} N3H → X^{5} N^{2}H; and g, X^{5} N1H → X^{5} N^{2}H. (C) Duplex containing the *S*-cdG·dA base pair; NOE cross-peaks are assigned as follows: h, A^{19} H2 → G^{7} N1H; i, C^{4} N^{4}H2 → G^{21} N1H; and j, C^{4} N^{4}H1 → G^{21} N1H.

$^{3}J_{H1'-H2''}$ were 5.3 and 8.8 Hz, respectively. With the exception of the terminal nucleotides, the $^{3}J_{H1'-H2'}$ for other nucleotides were 8−10 Hz, and the $^{3}J_{H1'-H2''}$ were 5−7 Hz. The ^{3}J coupling constants for the deoxyribose protons are tabulated in Table S2 in the Supporting Information.

Phosphodiester Backbone Conformation. The ^{31}P resonances were assigned from a ^{31}P−H3′ HMBC spectrum. With the exception of X^{5}, each exhibited heteronuclear coupling with H3′ of the 5′-neighbor nucleotide. The ^{31}P NMR spectrum of the *S*-cdG containing duplex was compared with the unmodified mismatched duplex (Figure S2 in the Supporting Information). At the *S*-cdG nucleotide, the ^{31}P resonance shifted upfield. The other ^{31}P resonances were clustered within a modest chemical shift range, centered in the spectral region characteristic of B-DNA.

Chemical Shift Perturbations. Chemical shifts of the non-exchangeable protons between the *S*-cdG-containing duplex and the unmodified mismatched duplex were compared (Figure 5). Remarkable changes were observed at X^{5} and the 5′- and 3′-neighboring nucleotides of the modified strand. C^{4} H2″ shifted downfield by 0.72 ppm; X^{5} H2′ and H2″ shifted upfield by 0.21 and 0.51 ppm, respectively; and T^{6} H6, H1′, and H2′ shifted downfield by 0.32, 0.24, and 0.23 ppm, respectively. The chemical shift perturbations for the complementary strand were small, with the exception of A^{19} H8 and T^{20} H1′, which shifted upfield by 0.24 and 0.31 ppm, respectively.

dx.doi.org/10.1021/tx2005053 | *Chem. Res. Toxicol.* 2012, 25, 478−490

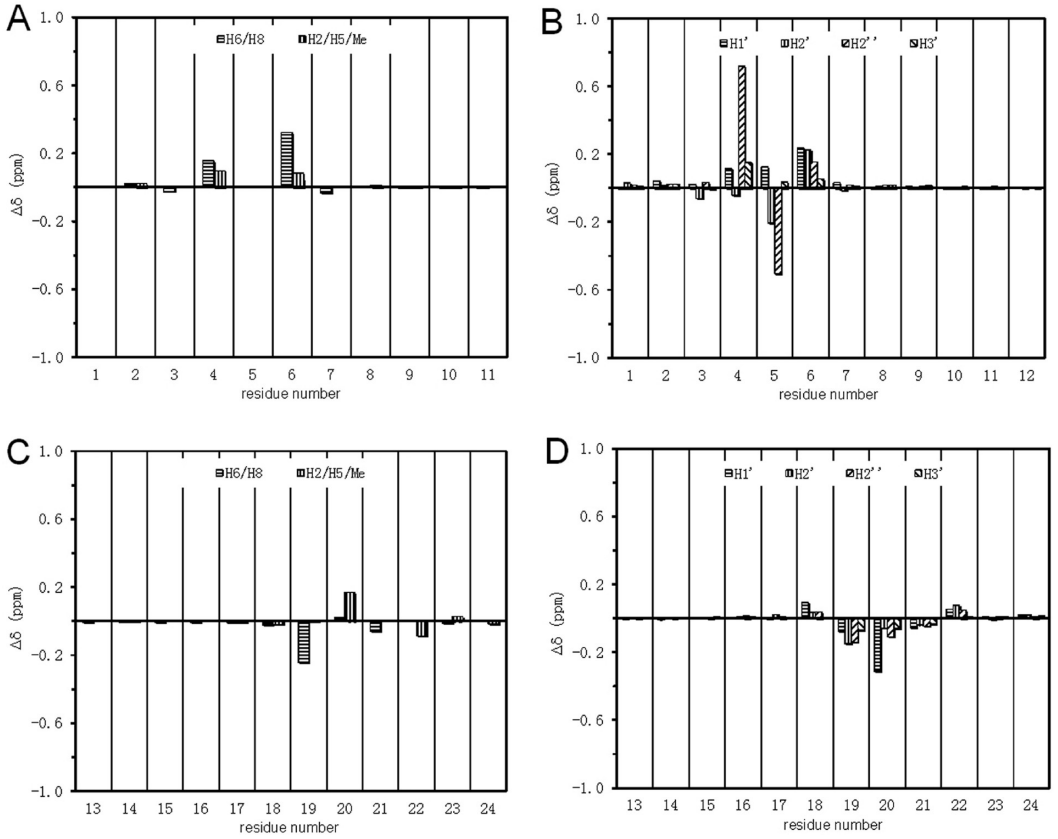

Figure 5. Chemical shift perturbations of the duplex containing the *S*-cdG·dT base pair. (A) Base protons of the modified strand. (B) 2′-Deoxyribose protons of the modified strand. (C) Base protons of the complementary strand. (D) 2′-Deoxyribose protons of the complementary strand.

Structural Refinement. A total of 406 distance restraints, including 263 intranucleotide and 143 internucleotide restraints, were calculated from the intensities of NOE cross-peaks (Table S3 in the Supporting Information).[45] A total of 21 NOEs involving the *S*-cdG protons were used as restraints. A total of 47 empirical distance restraints arising from Watson–Crick base pairing were used, as were 160 empirical torsion angle restraints that were applied to the nonterminal nucleotides. These were justified based upon NMR data, which suggested that structural perturbations were localized at and adjacent to the lesion site. Weak wobble base pair restraints were used for the X^5·T^{20} base pair, and no torsion angle restraints were used for the C^4·G^{21}, X^5·T^{20}, and T^6·A^{19} base pairs. The restraints are summarized in Table 1.

The rMD calculations for the *S*-cdG-containing duplex were performed from A and B form starting structures. Ten emergent structures, five each for A- and B-DNA starting structures, were obtained and minimized with respect to potential energy. All converged as indicated by pairwise rmsd comparisons (Table 1). The accuracies of the emergent structures were evaluated by comparison of theoretical NOE intensities for the refined structure calculated by the program CORMA[44] to the experimental NOE intensities, to yield sixth root residuals (R_1^x).[42] These, as well as the residuals for intra- or internucleotide NOEs, were consistently <0.1 (Table 1). R_1^x values for each nucleotide were <0.15 (Figure S3 in the Supporting Information). Thus, the refined structures provided accurate depictions of the NOE data.

Structure of the S-cdG:dT Mispair. The X^5·T^{20} pair adopted the wobble conformation (Figure 6). Figure 7A,B shows base stacking and base pairing at the lesion site. The X^5·T^{20} pair exhibited a shift of −0.8 Å, displacing C^4 toward the major groove. This pair exhibited a greater than normal opening of 16.8°. Typical B-DNA pairing and stacking interactions were maintained for the remaining base pairs (Table S4 in the Supporting Information). The *S*-cdG deoxyribose was in the O4′-*exo*, "west" pseudorotation (Figure 8A), with P = 280° and τ_m = 47°. The heavy atoms N9, O3′, and C5′ were axial about the deoxyribose ring. The complementary T^{20} was in the

Table 1. rMD Restraints and Statistical Analysis of rMD Converged Structures of the *S*-cdG Containing Duplexes

duplex	*S*-cdG·dT	*S*-cdG·dA
total restraints for rMD calculation	613	607
experimental NOE distance restraints	406	399
intranucleotide NOE restraints	263	260
internucleotide NOE restraints	143	139
S-cdG NOE restraints	21	30
empirical base pair restraints	47	43
empirical torsion angle restraints	160	165
backbone torsion angle restraints	90	95
deoxyribose torsion angle restraints	70	70
structure statistics[a]		
NMR R factor (R_1^x) ($\times 10^{-2}$)	6.12	6.85
intranucleotide NOEs	5.33	6.45
internucleotide NOEs	7.76	7.67
rmsd deviation of refined structures	0.52	0.44

[a]Mixing time used to calculate R_1^x was 250 ms. $R_1^x = \sum|(a_0)_i^{1/6} - (a_c)_i^{1/6}|/|(a_0)_i^{1/6}|$, where a_0 and a_c are the intensities of observed (nonzero) and calculated NOE cross-peaks, respectively.

dx.doi.org/10.1021/tx2005053 | *Chem. Res. Toxicol.* 2012, 25, 478–490

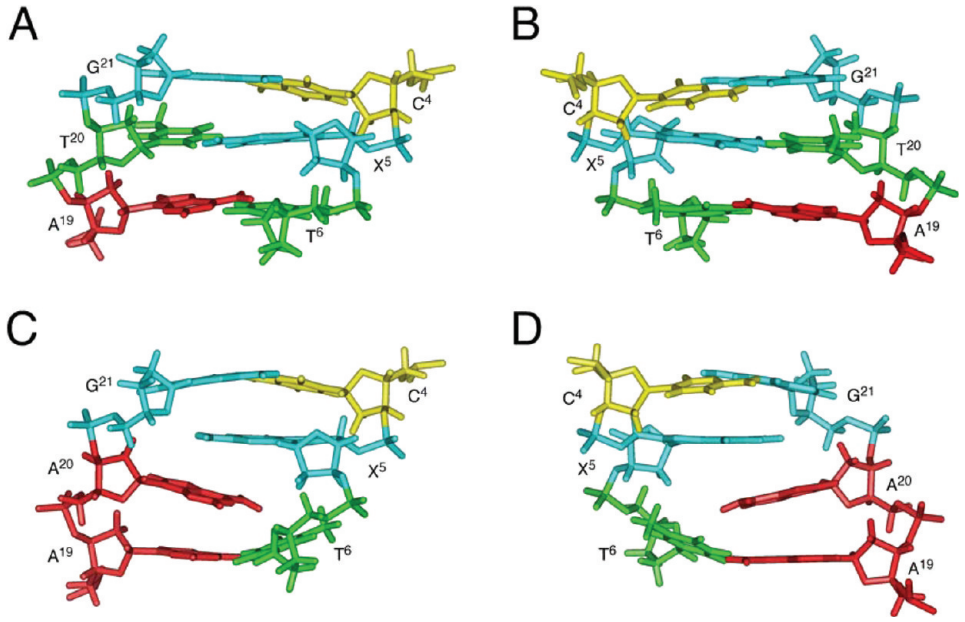

Figure 6. Expanded views of the refined structure of the *S*-cdG containing duplexes at the lesion site. (A) Duplex containing the *S*-cdG·dT base pair, viewed from the minor groove. (B) Duplex containing the *S*-cdG·dT base pair, viewed from the major groove. (C) Duplex containing the *S*-cdG·dA base pair, viewed from the minor groove. (D) Duplex containing the *S*-cdG·dA base pair, viewed from the major groove.

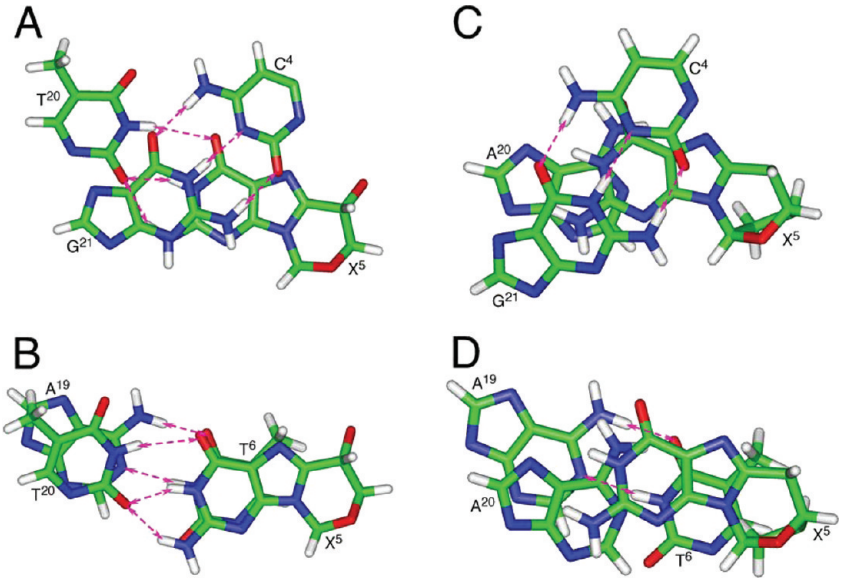

Figure 7. Base pairing and base stacking of the refined structures of the *S*-cdG containing duplex at the lesion site. The pink arrows indicate anticipated hydrogen-bonding interactions. (A) The C^4·G^{21} and X^5·T^{20} base pairs. (B) The X^5·T^{20} and T^6·A^{19} base pairs. (C) The C^4·G^{21} and X^5·A^{20} base pairs. (D) The X^5·A^{20} and T^6·A^{19} base pairs.

C4′-*exo*, "north" pseudorotation, with P = 65° and τ_m = 37°. Consequently, X^5 H2″ was farther from the X^5 purine ring as compared to the H2″ protons in B-DNA, and C4 H2″ was proximate to the X^5 purine ring. With the exception of the terminal nucleotides, other pseudorotations were either C1′-*exo* or C2′-*endo*. The six-membered ring C8–N9–C1′–O4′–C4′–C5′ adopted the envelope (half boat) conformation. Helicoidal analysis of the backbone torsion angles (Figure S4 in the Supporting Information) showed that for *S*-cdG, the β angle shifted from 180 to −78°. The γ angle shifted from 50 to −57°. Perturbations of the δ and ζ torsion angles from 120 to 147° and from −90 to −58°, respectively, were also observed. There was also a change for the N-glycosidic torsion angle χ from −120 to −162°. For the complementary T^{20}, a perturbation of the δ torsion angle from 120 to 83° was observed.

S-cdG Mismatched with dA. *NMR Resonance Assignments.* The nonexchangeable protons were assigned based upon the sequential connectivity of the base proton H6 or H8 dipolar couplings with H1′ deoxyribose protons (Figure 2C,D).[59,60] For the modified strand, the NOE connectivity was observed from G^1 to C^4. The connectivity exhibited an interruption at X^5 due to the lack of a proton at the C8 carbon. The X^5 H1′ proton was identified at 6.12 ppm; it exhibited a weak X^5 H1′ → T^6 H6 NOE, suggesting that the distance between these two protons was greater than in B-DNA. The sequential connectivity resumed from T^6 to T^{12}. For the modified strand,

dx.doi.org/10.1021/tx2005053 | *Chem. Res. Toxicol.* 2012, 25, 478–490

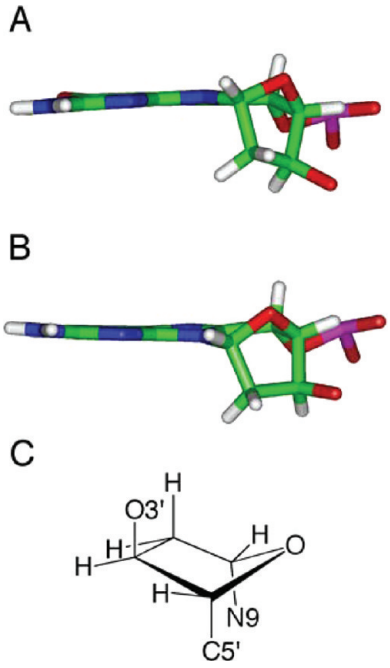

Figure 8. Deoxyribose conformations of the *S*-cdG in the refined structures. (A) Duplex containing the *S*-cdG·dT base pair. (B) Duplex containing the *S*-cdG·dA base pair. (C) O4′-*exo* pseudorotation of the deoxyribose.

the deoxyibose H1′ protons were observed within a narrow chemical shift window, between 5.8 and 6.3 ppm. The complete sequential connectivity was observed for the complementary strand.

The resonances of A^{19} H2 and A^{20} H2 appeared at 7.41 and 7.46 ppm, respectively. An NOE was observed between them. In addition, A^{19} H2 exhibited an NOE with G^{7} N1H (Figure 4C), suggesting both A^{19} and A^{20} were intercalated. As expected, both H2 protons exhibited NOEs with H1′ protons in the minor groove (Figure 9). Notably, A^{20} exhibited NOEs with both T^{6} H1′ and A^{19} H1′ of the 5′-flanking T^{6}·A^{19} base pair but did not exhibit NOEs with C^{4} H1′ or G^{21} H1′ of the 3′-flanking C^{4}·G^{21} base pair.

The assignments of X^{5} deoxyribose protons were made by analysis of scalar and dipolar couplings. Figure 3B displays a tile plot derived from a NOESY spectrum at 60 ms mixing time. X^{5} H1′ exhibited dipolar couplings with H2′ and H2″; weak scalar couplings were also observed. H3′ exhibited dipolar couplings with H2′, H2″, and H4′, whereas the scalar couplings were not observed. H4′ exhibited both scalar and dipolar couplings with the H5′ proton. For the remainder of the duplex, the H2′, H2″, H3′, and H4′ resonances were assigned unequivocally. The absolute configurations of the geminal H2′ and H2″ protons were assigned from their NOEs to H1′ and H3′. With the exception of the unresolved resonances for G^{11}, T^{12}, and C^{24}, H2′ exhibited a weaker NOE with H1′ than did H2″, whereas it exhibited a stronger NOE with H3′ than did H2″. The resonance assignments of the nonexchangeable DNA protons are tabulated in Table S5 in the Supporting Information.

The resonances of the base imino protons were assigned based on sequential connectivity in NOESY spectra and NOEs to the amino protons of Watson−Crick base pairs (Figure 4C).[61] The NOE connectivity was observed from $T^{2} \rightarrow G^{3}$ to G^{21} and from $G^{7} \rightarrow T^{8} \rightarrow T^{9} \rightarrow T^{10}$ to G^{11}. The resonances of X^{5} N1H and T^{6} N3H were not assigned although a broad resonance was

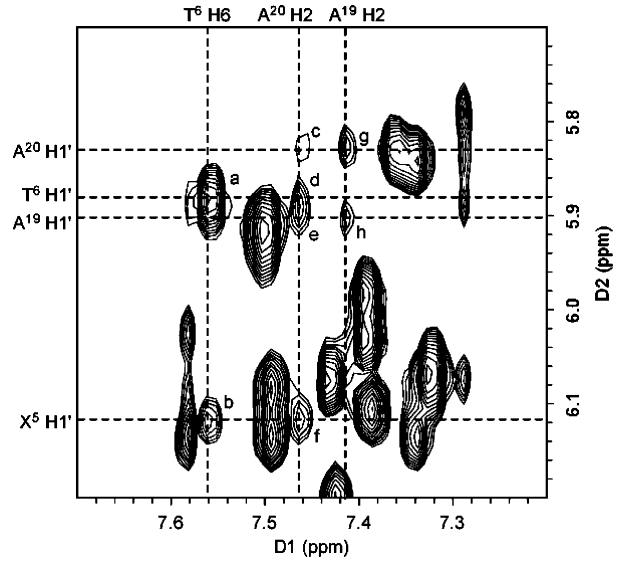

Figure 9. Expansion of the NOESY spectrum (250 ms) of the duplex containing the *S*-cdG·dA base pair showing the intercalation of A^{19} and A^{20}. NOE cross-peaks are assigned as follows: a, T^{6} H6 → T^{6} H1′; b, T^{6} H6 → X^{5} H1′; c, A^{20} H2 → A^{20} H1′; d, A^{20} H2 → T^{6} H1′; e, A^{20} H2 → A^{19} H1′; f, A^{20} H2 → X^{5} H1′; g, A^{19} H2 → A^{20} H1′; and h, A^{19} H2 → A^{19} H1′.

observed at ∼13.2 ppm at temperatures below 15 °C. The assignment failed due to a lack of NOE interactions. At the 5′-neighbor base pair, G^{21} N1H exhibited NOEs with C^{4} N^{4} H1 and N^{4} H2. With the exception of the terminal base pairs, the remaining NOE cross-peaks arising from Watson−Crick hydrogen bonding were observed.

Deoxyribose Coupling Constants. The scalar couplings of the 2′-deoxyribose H1′ protons with the H2′ and H2″ protons were measured from an E-COSY spectrum (Figure S1 in the Supporting Information). The $^{3}J_{H1'-H2'}$ and $^{3}J_{H1'-H2''}$ values for X^{5} were 2.7 and 7.2 Hz, respectively. The $^{3}J_{H4'-H5'}$ was 6.7 Hz, whereas the $^{3}J_{H3'-H4'}$ was not measurable. With the exception of the terminal nucleotides, the $^{3}J_{H1'-H2'}$ for other nucleotides were 8−10 Hz, and the $^{3}J_{H1'-H2''}$ were 5−7 Hz. The ^{3}J coupling constants for the deoxyribose protons are tabulated in Table S6 in the Supporting Information.

Phosphodiester Backbone Conformation. The ^{31}P resonances were assigned from a ^{31}P−H3′ HMBC spectrum. With the exception of X^{5}, each exhibited a heteronuclear coupling with H3′ of the 5′-neighbor nucleotide. The spectrum of the *S*-cdG-containing duplex was compared with the unmodified mismatched duplex (Figure S2 in the Supporting Information). At the modified nucleotide, the ^{31}P resonance shifted upfield. The other ^{31}P resonances were clustered within a modest chemical shift range, in the spectral region characteristic of B-DNA.

Structural Refinement. A total of 399 distance restraints, including 260 intranucleotide and 139 internucleotide restraints were calculated from the intensities of NOE cross-peaks (Table S7 in the Supporting Information).[45] A total of 30 NOEs involving the *S*-cdG protons were used as restraints. A total of 43 empirical distance restraints arising from Watson−Crick base pairing interactions were used, as were 165 empirical torsion angle restraints that were applied to refine the nonterminal nucleotides. These were justified based upon NMR data, which suggested that structural perturbations were localized at and adjacent to the lesion site. The data suggested that no base pairing existed at the X^{5}·A^{20} and T^{6}·A^{19} base pairs, so base pairing restraints

dx.doi.org/10.1021/tx2005053 | *Chem. Res. Toxicol.* 2012, 25, 478−490

were not used for these base pairs. No torsion angle restraints were used for the $C^4{\cdot}G^{21}$, $X^5{\cdot}A^{20}$, and $T^6{\cdot}A^{19}$ base pairs. The restraints used for the structure refinement are summarized in Table 1.

Ten rMD calculations, five each for A- and B-DNA starting structures, were performed. The 10 emergent structures were minimized with respect to potential energy. All converged as indicated by pairwise rmsd comparisons (Table 1). The accuracies of the emergent structures were evaluated by comparison of theoretical NOE intensities calculated for the refined structure by the program CORMA[44] to the experimental NOE intensities to yield sixth root residuals (R_1^x).[42] These, as well as the residuals for intra- or internucleotide NOEs, were consistently less than 0.1 (Table 1). R_1^x values for each nucleotide were less than 0.15 (Figure S3 in the Supporting Information). Thus, the refined structures provided accurate depictions of the NOE data.

Structure of the S-cdG:dA Mispair. Both X^5 and A^{20} intercalated into the duplex (Figure 6). Consequently, the helical rise values from $C^4{\cdot}T^{21}$ to $X^5{\cdot}A^{20}$ and from $X^5{\cdot}A^{20}$ to $T^6{\cdot}A^{21}$ were greater than normal, 5.4 and 4.6 Å, respectively. Figure 7C,D shows the base stacking and base pairing at the lesion site. Significant perturbations in shift were observed from base pairs $T^2{\cdot}A^{23}$ to $G^7{\cdot}A^{18}$, centered at the $X^5{\cdot}A^{20}$ base pair. The $C^4{\cdot}T^{21}$ base pair exhibited a greater than normal base pair twist of 54°. The remaining base pairs exhibited normal base stacking (Table S8 in the Supporting Information). The *S*-cdG nucleotide was in the O4′-*exo*, "west" pseudorotation (Figure 8B), with P = 264° and τ_m = 47°. The heavy atoms N9, O3′, and C5′ were axial about the deoxyribose ring. Consequently, X^5 H2″ was farther from the X^5 purine ring as compared to the H2″ protons in B-DNA, while C4 H2″ was proximate to the X^5 purine ring. With the exception of the terminal nucleotides, all other pseudorotations were either C1′-*exo* or C2′-*endo*. The six-membered ring C8−N9−C1′−O4′−C4′−C5′ adopted the envelope (half boat) conformation. Helicoidal analysis of the backbone torsion angles (Figure S4 in the Supporting Information) showed that at the lesion site, the β angle shifted from the characteristic 180 to −83°. The γ angle shifted from 50 to −59°. Perturbations of the δ and ζ torsion angles from 120 to +157° and from −90 to −75°, respectively, were also observed. There was also a change for the N-glycosidic torsion angle χ from −120 to −143°.

DISCUSSION

This work extends an investigation of oligodeoxynucleotides containing the *S*-cdG lesion.[34] If not repaired, *S*-cdG blocks DNA replication in *E. coli* and is genotoxic.[24] In SOS-induced *E. coli*, a mutation frequency of 34% is observed. Most mutations are *S*-cdG → A transitions, although *S*-cdG → T transversions and a deletion of the 5′-neighbor C are also observed.[24] Accordingly, structures in which *S*-cdG is placed opposite dT or dA, representing intermediates leading to *S*-cdG → A transitions and *S*-cdG → T transversions, are of interest.

Structure of the *S*-cdG:dT Mispair. The dG:dT mismatch often exists as a wobble base pair with both bases in the anti conformation. One might predict that locking *S*-cdG into the anti conformation about the N-glycosidic bond would be consistent with the formation of a wobble *S*-cdG:dT mismatch pair, and this appears to be the case. The formation of a wobble pair is consistent with the upfield shift of the X^5 N1H resonances, which was also observed for the G^5 N1H of the corresponding unmodified duplex (Figure 1B).[62−66] However, the T^{20} N3H resonance was not observed, indicating enhanced solvent exchange at the *S*-cdG·dT wobble pair. The structural refinement suggests the potential formation of a three-point hydrogen bond among X^5 N1H, X^5 N^2H2, and T^{20} O^2 and a weak hydrogen bond between X^5 O^6 and T^{20} N3H (Figure 7). However, the observation that the *S*-cdG·dT wobble pair exhibits a T_m 5 °C lower than the corresponding duplex containing a dG·dT mismatch pair (Figure 1A) suggests that the incorporation of *S*-cdG reduces the stability of dG·dT wobble pairing. The broadening of the T^6 N3H and T^{20} N3H resonances as compared to the other thymine imino resonances (Figure 1B) suggests that the greatest destabilization occurs at the modified $X^5{\cdot}T^{20}$ and 3′-neighboring $T^6{\cdot}A^{19}$ base pairs. The 5′-neighboring $C^4{\cdot}G^{21}$ base pair is mildly affected. The base pair shifts at the $C^4{\cdot}G^{21}$ and $X^5{\cdot}T^{20}$ base pairs are consistent with this conclusion. Similarly, for the *S*-cdG:dC pairing interaction, a 9 °C decrease in T_m was observed relative to the unmodified duplex.[34] The thermal destabilization of this duplex is likely associated with the shift of the *S*-cdG deoxyribose to the O4′-*exo* (west) pseudorotation, as opposed to the "south" pseudorotation (C2′-*endo*) observed in B-DNA or the "north" pseudorotation (C3′-*endo*) in A-DNA.[51,67] Moreover, the complementary T^{20} deoxyribose shifts to the C4′-*exo* (north) pseudorotation, as evidenced by the $^3J_{H1'\text{-}H2'}$ and $^3J_{H1'\text{-}H2''}$ of 5.3 and 8.8 Hz, respectively (Table S2 in the Supporting Information). The accommodation of the constrained *S*-cdG nucleotide necessitates helicoidal perturbation of the phosphodiester backbone torsion angles β, γ, δ, and ζ in the modified strand. Additionally, smaller perturbations of the T^{20} phosphodiester backbone torsion angle δ in the complementary strand (Figure S4 in the Supporting Information) may factor in the reduced stability of the *S*-cdG·dT vs dG·dT mispairing interaction.

S-cdG:dA Mispair. Both *S*-cdG and dA are inserted into the duplex, but they do not engage in hydrogen bonding. Instead, helicoidal perturbations of the modified strand allow both to intercalate, creating a gap at the mismatched region. The absence of the G^{21} N1H → A^{20} H2 NOE agrees with the gap between A^{20} and G^{21} caused by the intercalation of *S*-cdG (Figure 6C,D). This is also consistent with the observation that A^{20} H2 exhibits NOEs with both H1′ protons of the 3′-flanking $T^6{\cdot}A^{19}$ pair, but not with the H1′ protons of the 5′-flanking $C^4{\cdot}G^{21}$ pair, suggesting A^{20} was close to $T^6{\cdot}A^{19}$ but further from $C^4{\cdot}G^{21}$ (Figure 9). The observation of the A^{19} H2 → A^{20} H2 NOE suggests A^{20} remains intercalated. The 8 °C decrease of the T_m as compared to the duplex containing a dG·dA mispair is probably related to alterations of the *S*-cdG phosphodiester backbone torsion angles β, γ, δ, and ζ and to perturbations of the base pair shift parameters at the $C^4{\cdot}G^{21}$ and $X^5{\cdot}A^{20}$ base pairs, which are necessitated to accommodate the constrained *S*-cdG O4′-*exo* (west) pseudorotation. It is of interest to note that Malyshev et al.[68] obtained a similar structure for a "self-intercalating" non-natural, non-hydrogen-bonding base pair that demonstrates excellent polymerase activity, with slower rates of extension.

The *S*-cdG·dA mismatch is distinct from the dG·dA mismatch as dG·dA mismatch pairs are influenced by sequence and pH. The failure to observe the imino resonances for base pairs $C^4{\cdot}G^{21}$, $X^5{\cdot}A^{20}$, and $T^6{\cdot}A^{19}$ of the unmodified duplex is consistent with this notion and suggests an increased rate of exchange of these protons with solvent, perhaps accompanied by structural disorder. A dG(anti)·dA(anti) pair was identified by Prive et al.[69,70] The dG(anti)·dA(syn) pair has been identified in the crystalline state at pH > 7,[71−73] while the

dx.doi.org/10.1021/tx2005053 | *Chem. Res. Toxicol.* 2012, 25, 478−490

protonated dG(syn)·dA$^+$(anti) pair has been identified at pH 6.6.[74,75] In solution, the dG(anti)·A(anti) pair is observed at neutral or basic pH conditions.[76−80] The dG(syn)·dA$^+$(anti) base pair is observed at acidic pH.[80,81] Carbonnaux et al.[80] observed that the latter is stabilized by bifurcated hydrogen bonds. Another type of dG(anti)·dA(anti) pairing is associated with tandem dG:dA mismatches.[78,82−84] This is referred to as a "sheared" or "type I1" G(anti)·A(anti) base pair and is accompanied by phosphodiester backbone perturbations. These differences between the S-cdG·dA and dG·dA mismatches are attributed to the fact that the *S*-cdG lesion is locked into the anti conformation about the N-glycosidic bond and the shift of the deoxyribose to the O4′-*exo* (west) pseudorotation. The dA(anti)·dG(anti) "face-to-face" conformation[69,70,76−78,80,82−87] would predict an NOE between G^{21} N1H and A^{20} H2, which is not observed (Figure 4C).

Structure−Activity Relationships. The wobble *S*-cdG·dT pair (Figure 6) is consistent with the site-specific mutagenesis studies in SOS-induced *E. coli*, showing a preponderance of *S*-cdG → dA transition mutations.[24] Because low levels of S-cd G → dT transversions are observed in *E. coli*,[24] we surmise that low levels of dATP are incorporated opposite *S*-cdG during trans-lesion synthesis. It has been suggested that Klenow DNA polymerases insert dATP opposite *S*-cdG.[25] Further studies of template·primers containing the *S*-cdG lesion complexed with error-prone polymerases will be of interest. The low levels of *S*-cdG → dT transversions might reflect the distortion of the *S*-cdG·dA mismatch, in which both *S*-cdG and dA are intercalated but do not hydrogen bond (Figure 6). Malyshev et al.[68] have reported that a non-natural, non-hydrogen-bonding base pair exhibiting a similar structure in duplex DNA demonstrates excellent polymerase activity, with slower rates of extension.

CONCLUSIONS

The structures of *S*-cdG placed opposite dA or dT were determined and compared with the structure when *S*-cdG placed opposite dC.[34] The *S*-cdG·dT base pair adopted a hydrogen-bonded wobble conformation, while the S-cdG·dA base pair differed from dG·dA mispairs—both *S*-cdG and dA were intercalated, but no hydrogen bonding was observed. In each instance, the *S*-cdG deoxyribose adopted the O4′-exo (west) pseudorotation and was accommodated by backbone and base-pairing helicoidal perturbations. Collectively, these perturbations may be important in understanding the mutagenicity and genotoxicity of *S*-cdG.

ASSOCIATED CONTENT

Supporting Information

^{1}H chemical shifts of the duplex containing *S*-cdG·dT base pair (Table S1); ^3J coupling constants and deoxyribose pseudorotation of the duplex containing *S*-cdG·dT base pair (Table S2); NOE distance restraints for the duplex containing *S*-cdG·dT base pair (Table S3); base-pairing and base-stacking parameters of the duplex containing *S*-cdG·dT base pair (Table S4); ^{1}H chemical shifts of the duplex containing *S*-cdG·dA base pair (Table S5); ^3J coupling constants and deoxyribose pseudorotations of the duplex containing *S*-cdG·dA base pair (Table S6); NOE distance restraints for the duplex containing *S*-cdG·dA base pair (Table S7); base-pairing and base-stacking parameters of the duplex containing *S*-cdG·dA base pair (Table S8); expansions of ECOSY showing the scalar couplings of H1′ with H2′ and H2″ (Figure S1); ^{31}P NMR of the *S*-cdG-containing duplexes (Figure S2); nucleotide-by-nucleotide sixth root residuals for the refined structures (Figure S3); backbone torsion angles of the *S*-cdG-modified duplexes (Figure S4); COSY of the duplex containing *S*-cdG·dA base pair as compared to the related unmodified duplex (Figure S5). This material is available free of charge via the Internet at http://pubs.acs.org.

Accession Codes

Complete structure data and final coordinates were deposited in the Protein Data Bank (www.rcsb.org). PDB ID codes: 2LFX for the *S*-cdG placed opposite dT and 2LFY for the *S*-cdG placed opposite dA.

AUTHOR INFORMATION

Corresponding Author

*Tel: 615-322-2589. Fax: 615-322-7591. E-mail: michael.p.stone@vanderbilt.edu.

Funding

This work was supported by NIH Grants CA-55678 (M.P.S.) and ES-013324 (A.K.B.). The Vanderbilt Center in Molecular Toxicology is funded by NIH grant P30 ES-00267. The Vanderbilt-Ingram Cancer Center is funded by NIH grant P30 CA-068485. Vanderbilt University and NIH grant RR-05805 provided additional funding for NMR instrumentation.

ABBREVIATIONS

cdA, 8,5′-cyclo-2′-deoxyadenosine; cdG, 8,5′-cyclo-2′-deoxyguanosine; CORMA, complete relaxation matrix analysis; COSY, correlated spectroscopy; DFT, density functional theory; E-COSY, exclusive correlation spectroscopy; GB, generalized Born model; HMBC, heternuclear multiple bond correlation spectroscopy; NOE, nuclear Overhauser enhancement; NOESY, nuclear Overhauser effect spectroscopy; rMD, restrained molecular dynamics; rmsd, root-mean-square deviation; TOCSY, total correlation spectroscopy; TPPI, time-proportional phase increment

REFERENCES

(1) Cooke, M. S., Evans, M. D., Dizdaroglu, M., and Lunec, J. (2003) Oxidative DNA damage: Mechanisms, mutation, and disease. *FASEB J. 17*, 1195−1214.

(2) Dedon, P. C. (2008) The chemical toxicology of 2′-deoxyribose oxidation in DNA. *Chem. Res. Toxicol. 21*, 206−219.

(3) Keck, K. (1968) Bildung von cyclonucleotiden bei betrahlung wassriger losungen von purinnucleotiden. *Z. Naturforsch. B 23*, 1034−1043.

(4) Dizdaroglu, M. (1986) Free-radical-induced formation of an 8,5′-cyclo-2′-deoxyguanosine moiety in deoxyribonucleic acid. *Biochem. J. 238*, 247−254.

(5) Dizdaroglu, M., Dirksen, M. L., Jiang, H. X., and Robbins, J. H. (1987) Ionizing-radiation-induced damage in the DNA of cultured human cells. Identification of 8,5′-cyclo-2′-deoxyguanosine. *Biochem. J. 241*, 929−932.

(6) Dirksen, M. L., Blakely, W. F., Holwitt, E., and Dizdaroglu, M. (1988) Effect of DNA conformation on the hydroxyl radical-induced formation of 8,5′-cyclopurine 2′-deoxyribonucleoside residues in DNA. *Int. J. Radiat. Biol. 54*, 195−204.

(7) Chatgilialoglu, C., Bazzanini, R., Jimenez, L. B., and Miranda, M. A. (2007) (5′S)- and (5′R)-5′,8-cyclo-2′-deoxyguanosine: Mechanistic insights on the 2′-deoxyguanosin-5′-yl radical cyclization. *Chem. Res. Toxicol. 20*, 1820−1824.

(8) Jaruga, P., and Dizdaroglu, M. (2008) 8,5′-Cyclopurine-2′-deoxynucleosides in DNA: Mechanisms of formation, measurement, repair and biological effects. *DNA Repair (Amsterdam) 7*, 1413−1425.

(9) Boussicault, F., Kaloudis, P., Caminal, C., Mulazzani, Q. G., and Chatgilialoglu, C. (2008) The fate of C5′ radicals of purine nucleosides under oxidative conditions. *J. Am. Chem. Soc. 130*, 8377−8385.
(10) Chatgilialoglu, C., Ferreri, C., and Terzidis, M. A. (2011) Purine 5′,8-cyclonucleoside lesions: Chemistry and biology. *Chem. Soc. Rev. 40*, 1368−1382.
(11) Mariaggi, N., Cadet, J., and Teoule, R. (1976) Radical cyclization of 2′-deoxyadenosine in aqueous-solution subjected to γ-irradiation. *Tetrahedron 32*, 2385−2387.
(12) Raleigh, J. A., Kremers, W., and Whitehouse, R. (1976) Radiation chemistry of nucleotides: 8,5′-Cyclonucleotide formation and phosphate release initiated by hydroxyl radical attack on adenosine monophosphates. *Radiat. Res. 65*, 414−422.
(13) Fuciarelli, A. F., Shum, F. Y., and Raleigh, J. A. (1986) Stereoselective intramolecular cyclization in irradiated nucleic acids: *R*- and *S*-8,5′-Cycloadenosine in polyadenylic acid. *Biochem. Biophys. Res. Commun. 134*, 883−887.
(14) Chatgilialoglu, C., Guerra, M., and Mulazzani, Q. G. (2003) Model studies of DNA C5′ radicals. Selective generation and reactivity of 2′-deoxyadenosin-5′-yl radical. *J. Am. Chem. Soc. 125*, 3839−3848.
(15) Navacchia, M. L., Chatgilialoglu, C., and Montevecchi, P. C. (2006) C5′-adenosinyl radical cyclization. A stereochemical investigation. *J. Org. Chem. 71*, 4445−4452.
(16) Dizdaroglu, M., Jaruga, P., and Rodriguez, H. (2001) Identification and quantification of 8,5′-cyclo-2′-deoxy-adenosine in DNA by liquid chromatography/ mass spectrometry. *Free Radical Biol. Med. 30*, 774−784.
(17) Jaruga, P., Birincioglu, M., Rodriguez, H., and Dizdaroglu, M. (2002) Mass spectrometric assays for the tandem lesion 8,5′-cyclo-2′-deoxyguanosine in mammalian DNA. *Biochemistry 41*, 3703−3711.
(18) Kirkali, G., de Souza-Pinto, N. C., Jaruga, P., Bohr, V. A., and Dizdaroglu, M. (2009) Accumulation of (5′*S*)-8,5′-cyclo-2′-deoxyadenosine in organs of Cockayne syndrome complementation group B gene knockout mice. *DNA Repair (Amsterdam) 8*, 274−278.
(19) Jaruga, P., and Dizdaroglu, M. (2010) Identification and quantification of (5′*R*)- and (5′*S*)-8,5′-cyclo-2′-deoxyadenosines in human urine as putative biomarkers of oxidatively induced damage to DNA. *Biochem. Biophys. Res. Commun. 397*, 48−52.
(20) Rodriguez, H., Jaruga, P., Leber, D., Nyaga, S. G., Evans, M. K., and Dizdaroglu, M. (2007) Lymphoblasts of women with BRCA1 mutations are deficient in cellular repair of 8,5′-cyclopurine-2′-deoxynucleosides and 8-hydroxy-2′-deoxyguanosine. *Biochemistry 46*, 2488−2496.
(21) Jaruga, P., Xiao, Y., Nelson, B. C., and Dizdaroglu, M. (2009) Measurement of (5′*R*)- and (5′*S*)-8,5′-cyclo-2′-deoxyadenosines in DNA *in vivo* by liquid chromatography/isotope-dilution tandem mass spectrometry. *Biochem. Biophys. Res. Commun. 386*, 656−660.
(22) Brooks, P. J. (2008) The 8,5′-cyclopurine-2′-deoxynucleosides: Candidate neurodegenerative DNA lesions in xeroderma pigmentosum, and unique probes of transcription and nucleotide excision repair. *DNA Repair (Amsterdam) 7*, 1168−1179.
(23) Kirkali, G., Tunca, M., Genc, S., Jaruga, P., and Dizdaroglu, M. (2008) Oxidative DNA damage in polymorphonuclear leukocytes of patients with familial Mediterranean fever. *Free Radical Biol. Med. 44*, 386−393.
(24) Jasti, V. P., Das, R. S., Hilton, B. A., Weerasooriya, S., Zou, Y., and Basu, A. K. (2011) (5′*S*)-8,5′-Cyclo-2′-deoxyguanosine is a strong block to replication, a potent pol V-dependent mutagenic lesion, and is inefficiently repaired in *Escherichia coli*. *Biochemistry 50*, 3862−3865.
(25) Gasparutto, D., Bourdat, A. G., D'Ham, C., Duarte, V., Romieu, A., and Cadet, J. (2000) Repair and replication of oxidized DNA bases using modified oligodeoxyribonucleotides. *Biochimie 82*, 19−24.
(26) Jaruga, P., Theruvathu, J., Dizdaroglu, M., and Brooks, P. J. (2004) Complete release of (5′*S*)-8,5′-cyclo-2′-deoxyadenosine from dinucleotides, oligodeoxynucleotides and DNA, and direct comparison of its levels in cellular DNA with other oxidatively induced DNA lesions. *Nucleic Acids Res. 32*, e87.
(27) Belmadoui, N., Boussicault, F., Guerra, M., Ravanat, J. L., Chatgilialoglu, C., and Cadet, J. (2010) Radiation-induced formation of purine 5′,8-cyclonucleosides in isolated and cellular DNA: High stereospecificity and modulating effect of oxygen. *Org. Biomol. Chem. 8*, 3211−3219.
(28) Miaskiewicz, K., Miller, J. H., and Fuciarelli, A. F. (1995) Theoretical analysis of DNA intrastrand cross linking by formation of 8,5′-cyclodeoxyadenosine. *Nucleic Acids Res. 23*, 515−521.
(29) Karwowski, B. T. (2009) 5 ′,8-Cyclopurine-2 ′-deoxynucleosides: Molecular structure and charge distribution - DFT study in gaseous and aqueous phase. *J. Mol. Struct. Theochem. 915*, 73−78.
(30) Karwowski, B. T. (2010) Formation of 5′,8-cyclo-2′-deoxyadenosine in single strand DNA. Theoretical quantum mechanics study. *Org. Biomol. Chem. 8*, 1603−1609.
(31) Birnbaum, G. I., Cygler, M., Dudycz, L., Stolarski, R., and Shugar, D. (1981) Comparison of solid-state and solution conformations of *R*-epimer and *S*-epimer of 8,5′-cycloadenosine and their relevance to some enzymatic-reactions. *Biochemistry 20*, 3294−3301.
(32) Haromy, T. P., Raleigh, J., and Sundaralingam, M. (1980) Enzyme-bound conformations of nucleotide substrates - X-ray structure and absolute-configuration of 8,5′-cycloadenosine monohydrate. *Biochemistry 19*, 1718−1722.
(33) Karwowski, B. T. (2008) (5′*R*)-5′,8-Cyclo-2′-deoxyadenosine: NMR and DFT study of its influence on T(PO)cdA structure. *Tetrahedron: Asymmetry 19*, 2390−2395.
(34) Huang, H., Das, R. S., Basu, A., K., and Stone, M. P. (2011) Structure of (5′*S*)-8,5′-cyclo-2′-deoxyguanosine in DNA. *J. Am. Chem. Soc. 133*, 20357−20368.
(35) Griesinger, C., Sorensen, O. W., and Ernst, R. R. (1985) Two-dimensional correlation of connected NMR transitions. *J. Am. Chem. Soc. 107*, 6394−6396.
(36) Marion, D., and Wuthrich, K. (1983) Application of phase sensitive two-dimensional correlated spectroscopy (COSY) for measurements of ^{1}H-^{1}H spin-spin coupling constants in proteins. *Biochem. Biophys. Res. Commun. 113*, 967−974.
(37) Bruker Biospin, Inc. (2010) *TOPSPIN*, v. 3.1, Bruker Biospin, Inc., Billerica, MA.
(38) Goddard, T. D., and Kneller, D. G. (2006) *SPARKY* v. 3.113, University of California, San Francisco.
(39) Piotto, M., Saudek, V., and Sklenar, V. (1992) Gradient-tailored excitation for single-quantum NMR spectroscopy of aqueous solutions. *J. Biomol. NMR 2*, 661−665.
(40) Gorenstein, D. G. (1992) ^{31}P NMR of DNA. *Methods Enzymol. 211*, 254−286.
(41) Markley, J. L., Bax, A., Arata, Y., Hilbers, C. W., Kaptein, R., Sykes, B. D., Wright, P. E., and Wuthrich, K. (1998) Recommendations for the presentation of NMR structures of proteins and nucleic acids. IUPAC-IUBMB-IUPAB inter-union task group on the standardization of data bases of protein and nucleic acid structures determined by NMR spectroscopy. *J. Biomol. NMR 12*, 1−23.
(42) James, T. L. (1991) Relaxation matrix analysis of two-dimensional nuclear Overhauser effect spectra. *Curr. Opin. Struct. Biol. 1*, 1042−1053.
(43) Keepers, J. W., and James, T. L. (1984) A theoretical study of distance determinations from NMR - Two-dimensional nuclear Overhauser effect spectra. *J. Magn. Reson. 57*, 404−426.
(44) Borgias, B. A., and James, T. L. (1989) Two-dimensional nuclear Overhauser effect: Complete relaxation matrix analysis. *Methods Enzymol. 176*, 169−183.
(45) Borgias, B. A., and James, T. L. (1990) MARDIGRAS—A procedure for matrix analysis of relaxation for discerning geometry of an aqueous structure. *J. Magn. Reson. 87*, 475−487.
(46) Liu, H., Spielmann, H. P., Ulyanov, N. B., Wemmer, D. E., and James, T. L. (1995) Interproton distance bounds from 2D NOE intensities: Effect of experimental noise and peak integration errors. *J. Biomol. NMR 6*, 390−402.
(47) Salazar, M., Fedoroff, O. Y., Miller, J. M., Ribeiro, N. S., and Reid, B. R. (1993) The DNA strand in DNA:RNA hybrid duplexes is neither B-form nor A-form in solution. *Biochemistry 32*, 4207−4215.

(48) Wang, H., Zuiderweg, E. R. P., and Glick, G. D. (1995) Solution structure of a disulfide cross-linked DNA hairpin. *J. Am. Chem. Soc. 117*, 2981−2991.
(49) Geen, H., and Freeman, R. (1991) Band-selective radio-frequency pulses. *J. Magn. Reson. 93*, 93−141.
(50) Lankhorst, P. P., Haasnoot, A. G., Erkelens, C., and Altona, C. (1984) Carbon-13 NMR in conformational analysis of nucleic acid fragments. 3. The magnitude of torsional angle in d(TpA) from CCOP and HCOP NMR coupling constants. *Nucleic Acids. Res. 12*, 5419−5428.
(51) Arnott, S., and Hukins, D. W. L. (1972) Optimised parameters for A-DNA and B-DNA. *Biochem. Biophys. Res. Commun. 47*, 1504−1509.
(52) Frisch, M. J., Trucks, G. W., Schlegel, H. B., Scuseria, G. E., Robb, M. A., Cheeseman, J. R., Montgomery, J. A., Vreven, T., Kudin, K. N., Burant, J. C., Millam, J. M., Iyengar, S. S., Tomasi, J., Barone, V., Mennucci, B., Cossi, M., Scalmani, G., Rega, N., Petersson, G. A., Nakatsuji, H., Hada, M., Ehara, M., Toyota, K., Fukuda, R., Hasegawa, J., Ishida, M., Nakajima, T., Honda, Y., Kitao, O., Nakai, H., Klene, M., Li, X., Knox, J. E., Hratchian, H. P., Cross, J. B., Adamo, C., Jaramillo, J., Gomperts, R., Stratmann, R. E., Yazyev, O., Austin, A. J., Cammi, R., Pomelli, C., Pomelli, J., Ochterski, W., Ayala, P. Y., Morokuma, K., Voth, G. A., Salvador, P., Dannenberg, J. J., Zakrzewska, V. G., Daniels, A. D., Farkas, O., Rabuck, A. D., Raghavachari, K., and Ortiz, J. V. (2004) *GAUSSIAN 03*, Gaussian, Inc., Wallingford, CT.
(53) Kirkpatrick, S., Gelatt, C. D. Jr., and Vecchi, M. P. (1983) Optimization by simulated annealing. *Science 220*, 671−680.
(54) Case, D. A., Cheatham, T. E. 3rd, Darden, T., Gohlke, H., Luo, R., Merz, K. M. Jr., Onufriev, A., Simmerling, C., Wang, B., and Woods, R. J. (2005) The AMBER biomolecular simulation programs. *J. Comput. Chem. 26*, 1668−1688.
(55) Bashford, D., and Case, D. A. (2000) Generalized Born models of macromolecular solvation effects. *Annu. Rev. Phys. Chem. 51*, 129−152.
(56) Tsui, V., and Case, D. A. (2000) Theory and applications of the generalized Born solvation model in macromolecular simulations. *Biopolymers 56*, 275−291.
(57) Lavery, R., and Sklenar, H. (1988) The definition of generalized helicoidal parameters and of axis curvature for irregular nucleic acids. *J. Biomol. Struct. Dyn. 6*, 63−91.
(58) Lu, X. J., and Olson, W. K. (2003) 3DNA: A software package for the analysis, rebuilding and visualization of three-dimensional nucleic acid structures. *Nucleic Acids Res. 31*, 5108−5121.
(59) Reid, B. R. (1987) Sequence-specific assignments and their use in NMR studies of DNA structure. *Q. Rev. Biophys. 20*, 2−28.
(60) Patel, D. J., Shapiro, L., and Hare, D. (1987) DNA and RNA: NMR studies of conformations and dynamics in solution. *Q. Rev. Biophys. 20*, 35−112.
(61) Boelens, R., Scheek, R. M., Dijkstra, K., and Kaptein, R. (1985) Sequential assignment of imino- and amino-proton resonances in ^{1}H NMR spectra of oligonucleotides by two-dimensional NMR spectroscopy. Application to a *lac* operator fragment. *J. Magn. Reson. 62*, 378−386.
(62) McDowell, J. A., He, L., Chen, X., and Turner, D. H. (1997) Investigation of the structural basis for thermodynamic stabilities of tandem GU wobble pairs: NMR structures of $(rGGAGUUCC)_2$ and $(rGGAUGUCC)_2$. *Biochemistry 36*, 8030−8038.
(63) Sahasrabudhe, P. V., and Gmeiner, W. H. (1997) Solution structures of 5-fluorouracil-substituted RNA duplexes containing G-U wobble base pairs. *Biochemistry 36*, 5981−5991.
(64) Allawi, H. T., and SantaLucia, J. Jr. (1998) NMR solution structure of a DNA dodecamer containing single G:T mismatches. *Nucleic Acids Res. 26*, 4925−4934.
(65) Chen, X., McDowell, J. A., Kierzek, R., Krugh, T. R., and Turner, D. H. (2000) Nuclear magnetic resonance spectroscopy and molecular modeling reveal that different hydrogen bonding patterns are possible for G:U pairs: One hydrogen bond for each G:U pair in $r(GGCGUGCC)_2$ and two for each G:U pair in $r(GAGUGCUC)_2$. *Biochemistry 39*, 8970−8982.
(66) Lee, J. H., Park, C. J., Shin, J. S., Ikegami, T., Akutsu, H., and Choi, B. S. (2004) NMR structure of the DNA decamer duplex containing double T:G mismatches of cis-syn cyclobutane pyrimidine dimer: implications for DNA damage recognition by the XPC-hHR23B complex. *Nucleic Acids Res. 32*, 2474−2481.
(67) Saenger, W. (1984) *Principles of Nucleic Acid Structure*, Springer-Verlag, New York, NY.
(68) Malyshev, D. A., Pfaff, D. A., Ippoliti, S. I., Hwang, G. T., Dwyer, T. J., and Romesberg, F. E. (2010) Solution structure, mechanism of replication, and optimization of an unnatural base pair. *Chemistry 16*, 12650−12659.
(69) Prive, G. G., Heinemann, U., Chandrasegaran, S., Kan, L. S., Kopka, M. L., and Dickerson, R. E. (1987) Helix geometry, hydration, and G:A mismatch in a B-DNA decamer. *Science 238*, 498−504.
(70) Prive, G. G., Heinemann, U., Chandrasegaran, S., Kan, L. S., Kopka, M. L., and Dickerson, R. E. (1988) A mismatch decamer as a model for general-sequence B-DNA. *Struct. Express 2*, 27−47.
(71) Brown, T., Hunter, W. N., Kneale, G., and Kennard, O. (1986) Molecular structure of the G:A base pair in DNA and its implications for the mechanism of transversion mutations. *Proc. Natl. Acad. Sci. U.S.A. 83*, 2402−2406.
(72) Hunter, W. N., Brown, T., and Kennard, O. (1986) Structural features and hydration of d(C-G-C-G-A-A-T-T-A-G-C-G); a double helix containing two G:A mispairs. *J. Biomol. Struct. Dyn. 4*, 173−191.
(73) Webster, G. D., Sanderson, M. R., Skelly, J. V., Neidle, S., Swann, P. F., Li, B. F., and Tickle, I. J. (1990) Crystal structure and sequence-dependent conformation of the A:G mispaired oligonucleotide d(CGCAAGCTGGCG). *Proc. Natl. Acad. Sci. U.S.A. 87*, 6693−6697.
(74) Brown, T., Leonard, G. A., Booth, E. D., and Chambers, J. (1989) Crystal structure and stability of a DNA duplex containing A(anti):G(syn) base-pairs. *J. Mol. Biol. 207*, 455−457.
(75) Leonard, G. A., and Hunter, W. N. (1993) Crystal and molecular structure of d(CGTAGATCTACG) at 2.25 Å resolution. *J. Mol. Biol. 234*, 198−208.
(76) Kan, L. S., Chandrasegaran, S., Pulford, S. M., and Miller, P. S. (1983) Detection of a guanine X adenine base pair in a decadeoxyribonucleotide by proton magnetic resonance spectroscopy. *Proc. Natl. Acad. Sci. U.S.A. 80*, 4263−4265.
(77) Nikonowicz, E. P., and Gorenstein, D. G. (1990) Two-dimensional ^{1}H and ^{31}P NMR spectra and restrained molecular dynamics structure of a mismatched GA decamer oligodeoxyribonucleotide duplex. *Biochemistry 29*, 8845−8858.
(78) Nikonowicz, E. P., Meadows, R. P., Fagan, P., and Gorenstein, D. G. (1991) NMR structural refinement of a tandem G·A mismatched decamer $d(CCAAGATTGG)_2$ via the hybrid matrix procedure. *Biochemistry 30*, 1323−1334.
(79) Patel, D. J., Kozlowski, S. A., Ikuta, S., and Itakura, K. (1984) Deoxyguanosine-deoxyadenosine pairing in the d(C-G-A-G-A-A-T-T-C-G-C-G) duplex: Conformation and dynamics at and adjacent to the dG x dA mismatch site. *Biochemistry 23*, 3207−3217.
(80) Carbonnaux, C., Van Der Marel, G. A., Van Boom, J. H., Guschlbauer, W., and Fazakerley, G. V. (1991) Solution structure of an oncogenic DNA duplex containing a G·A mismatch. *Biochemistry 30*, 5449−5458.
(81) Gao, X., and Patel, D. J. (1988) G(syn)·A(anti) mismatch formation in DNA dodecamers at acidic pH: pH-Dependent conformational transition of G:A mispairs detected by proton NMR. *J. Am. Chem. Soc. 110*, 5178−5182.
(82) Li, Y., Zon, G., and Wilson, W. D. (1991) NMR and molecular modeling evidence for a G:A mismatch base pair in a purine-rich DNA duplex. *Proc. Natl. Acad. Sci. U.S.A. 88*, 26−30.
(83) Chou, S. H., Cheng, J. W., and Reid, B. R. (1992) Solution structure of $[d(ATGAGCGAATA)]_2$. Adjacent G:A mismatches stabilized by cross-strand base-stacking and BII phosphate groups. *J. Mol. Biol. 228*, 138−155.
(84) Maskos, K., Gunn, B. M., LeBlanc, D. A., and Morden, K. M. (1993) NMR study of G:A and A:A pairing in $(dGCGAATAAGCG)_2$. *Biochemistry 32*, 3583−3595.

(85) Patel, D. J., Kozlowski, S. A., Ikuta, S., and Itakura, K. (1984) Dynamics of DNA duplexes containing internal G:T, G:A, A:C, and T:C pairs: Hydrogen exchange at and adjacent to mismatch sites. *Fed. Proc. 43*, 2663−26707.

(86) Greene, K. L., Jones, R. L., Li, Y., Robinson, H., Wang, A. H., Zon, G., and Wilson, W. D. (1994) Solution structure of a GA mismatch DNA sequence, d(CCATGAATGG)$_2$, determined by 2D NMR and structural refinement methods. *Biochemistry 33*, 1053−1062.

(87) Boulard, Y., Cognet, J. A., Gabarro-Arpa, J., Le Bret, M., Carbonnaux, C., and Fazakerley, G. V. (1995) Solution structure of an oncogenic DNA duplex, the *K-ras* gene and the sequence containing a central C:A or A:G mismatch as a function of pH: Nuclear magnetic resonance and molecular dynamics studies. *J. Mol. Biol. 246*, 194−208.